−1−

CONF-850809--42

DE85 009717

Thermal Stress Analysis of Metal Basemat Concept

J. M. Kennedy
Reactor Analysis and Safety Division
Argonne National Laboratory
9700 South Cass Avenue
Argonne, Illinois 60439, U.S.A.

D. F. Schoeberle
Department of Mechanical Engineering
University of Illinois at Chicago
Chicago, Illinois 60680, U.S.A.

DISCLAIMER

Abstract

An analysis has been made of a proposed General Electric Company metal basemat concept employing the finite element program STRAW. The basemat is a cast low-carbon steel circular plate which is integral with a poured cavity wall. The integral basemat and cavity wall provides a barrier for core debris accommodation. A thermo-mechanical stress analysis of the unit was performed for several different thermal loadings. Integrity of the cavity wall is maintained if a cooling system is employed for the outer surface; if not, creep buckling failure is predicted.

1. Introduction

An analysis has been made of a proposed commercial company metal basemat concept shown in Fig. 1. The basemat is a cast (inplace) low-carbon steel circular plate of thickness three feet and is integral with a poured cavity wall that is eight inches thick. The integral basemat and cavity wall provides a barrier for core debris accommodation during a hypothetical core meltdown.

The specific task was to perform a thermal stress analysis of the unit for three different thermal loadings: (1) a short-term transient where the upper surface of the basemat is exposed to 900°C liquid sodium almost instantaneously, (2) a long-term transient where the basemat and cavity wall surface temperature increases from 540°C to 900°C in about a period of twenty hours, and (3) the identical long-term transient except that the outside cavity wall below the sodium level has a varying temperature condition where the temperature increases linearly from 100°C to 250°C in twenty hours and then is held at 250°C. For all tasks, the lower surface of the basemat was assumed to be held at 100°C by cooling pipes and solid supporting material beneath it. The outer layer of the cavity wall and the outermost top layer of the basemat were assumed to be perfectly insulated.

To study the effects of the driving mechanisms and/or possible design variation, the reactor assembly weight was removed from the cavity wall for two cases. A variation of reactor assembly weight loading and thermal boundary provides the several cases for study.

The coupled thermal and stress analysis implicit time integration cluster of the ANL/RAS STRAW [1,2] program was employed for this study along with the developed constitutive algorithm for plain low-carbon steel.

2a   Finite Element Model of Metal Basemat and Cavity Wall

A symmetric slice section through the proposed configuration is shown as Fig. 2. The finite-element mesh includes 38 elements of the axisymmetric thin-shell type and 39 nodal points with the numbering scheme shown on the figure.

The non-uniform temperature distributions through the walls shown in Fig. 2 are required both for a thermal stress analysis and for input to the creep rate equations. The STRAW code contains a built-in heat conduction module which can be used to solve the heat conduction equation simultaneously with the stress analysis. These thermal finite-element routines automatically generate the thermal analysis mesh and solve for the nodal temperatures [1,2]. In the problems reported here, each structural element was subdivided into ten thermal elements of the isoparametric quadrilateral type leading to a total of 380 thermal finite elements and 429 thermal nodes. The distribution of the thermal nodes is shown in Fig. 3.

The displacement boundary conditions applied at the shell nodes on Fig. 2 were chosen to simulate the physical nature of the restraints shown in Fig. 1. Node 1 was constrained due to symmetry to move only on the vertical centerline; nodes 10 and 36 were constrained by a roller-type support to simulate a vertical motion constraint; the upper node 39 was constrained by a side-roller support to prevent horizontal motion.

The material properties for this simulation are given in Table I. The weight of molten sodium is assumed to be 1700 tons, while that of the reactor configuration is 3330 tons.

3.   Constitutive Relationship for Low-Carbon Steel

Since the designated long-term transients (problems 2 and 3) were expected in advance to cause a considerable amount of creep in the low-carbon steel at 900°C, an algorithm developed by DiMelfi and Kramer [3] has been incorporated. This algorithm will be used as part of the constitutive law in the STRAW code to be able to provide temperature- and strain-rate dependent material properties. In particular, the flow stress and the plastic stress-strain law slope are calculated for a given temperature and strain rate. These values are then used to calculate the various stress components and total accumulated plastic strain for the given strain conditions.

However, DiMelfi and Kramer's work employs constants that are valid only for type 316 stainless steel. Parameterization was thus needed for performing a thermal shock and creep analysis where the structure is composed of plain, low-carbon steel. The constants in this temperature and strain-rate dependent stress-strain law were numerically fitted to temperature dependent material properties selected from the Metals Handbook [4]. The strain-rate dependent terms in their equations were fitted to the data of a creep experiment performed in England by Crossland, et al [5].

This process of revising the DiMelfi and Kramer constitutive equation to fit the data for plain, low-carbon steel is necessary in order to consider creep effects in long-term problems by using equivalent viscoplasticity theory. As a result of this extensive numerical fitting process, the necessary constants were obtained: (the role of these constants is explained in Ref. 3).

This developed constitutive relation was tested by modeling actual creep experiments. The experiments chosen for verification of the above parameters were performed at the University of Kyoto in Japan by Taira and Ohtani [6]. The code calculation results agreed well with the experimental values of thermo-mechanical loaded tubular specimens.

4. Results

4.1 Short-Term Transient

The short-time rapid transient problem (1) is intended to simulate the accident whereby some hot sodium is suddenly dumped on the upper surface of the basemat. This case was modeled with a time step of $\Delta t = 10.0$ s. The thermal boundary conditions were expressed by a ramp-type rise up to the hot temperature of 900°C in five time steps, after which the temperature was held constant until thermal equilibrium was ensured. The hot temperature was applied to load line 1 on Fig. 3, load lines 2 and 3 were held at the initial cold temperature of 100°C, all remaining thermal boundary lines were assumed to be perfectly insulated.

The weight of the eight-inch thick vertical cavity wall was included as an equivalent concentrated force acting vertically on each node shown in Fig. 2. In addition to this load, we assumed the cavity wall supports the reactor configuration plus sodium weighing 5030 tons; this extra load was included as an equivalent concentrated force on node 39 of Fig. 2.

The calculated results for this problem are not very severe. The maximum value of the total accumulated plastic strain occurred on the inner surface of the cavity wall at the junction with the basemat and reached the steady state-value of 3.26%. The total effective stress reached an equilibrium value of 9.62 MPa at steady state. The increase in the vertical displacement at the basemat centerline is 0.034 meters.

4.2 Long-Term Transient

Results are to be obtained where part of the structure is to be subjected to a slow temperature rise, from 540°C to 900°C in about twenty hours and then held at 900°C. The set of five cases consists of three variations in the structural modeling and two variations of the thermal boundary conditions on thermal load line 5 on Fig. 3. A summary of the major results is included as Table II.

The hot temperature was applied to thermal load lines 1 and 6 shown in Fig. 3. We thus assumed the hot sodium had sufficient time to pile up on the inner part of the basemat. The remaining thermal load lines shown in Fig. 3 were treated exactly as before except for the variation of load line 5.

Two variations in structural modeling were considered employing thermal loading condition [2]. In problem (2a), the same four nodes were constrained as before, while the weight of 1700 tons of molten sodium and core debris was included as an equivalent downward pressure on finite elements 1 through 9. The linearly varying lateral pressure acting on the cavity wall was also accounted for by pressurizing elements 23 through 30. The weight of the cavity wall and reactor parts (3330 tons) was included.

In problem (2b), the same gradual rise in temperature and pressure were used, but shell nodes 1 through 10 in Fig. 2 were constrained to prevent vertical motions. The downward force of molten sodium is then irrelevant in problem (2b) since the shell nodes cannot displace in the direction of the weight.

The calculated results for problems (2a) and (2b) are very similar. The radial-displacement of structural nodes 13 and 15 (see Fig. 2) has exceeded one meter in magnitude, whereas the wall itself is only 0.2032 meters thick. These results show that the linearly varying lateral pressure due to the height of the static sodium liquid zone is sufficient to

buckle the cavity wall. With the adiabatic thermal boundary condition on the outer surface of the cavity wall, the wall can heat up to a nearly uniform temperature throughout the thickness. The material properties of the cavity wall are drastically reduced as the temperature approaches 900°C, and the wall does not have sufficient integrity to overcome the buckling phenomena.

Proposed case (2c) is intended to simulate a slightly different structural design, whereby the weight of the reactor assembly would be supported by an external structure apart from the basemat concept. Therefore, the concentrated load carried by structural node 39 of Fig. 2 was reduced to zero in this calculation. The sodium weight of 1700 tons was maintained on the basemat, and the adiabatic thermal boundary condition on the outer cavity wall surface was maintained.

This problem survived the fifty-hour calculation time period used, but the trend of the results is too similar to those of case (2a). In particular, the total radial displacement of structural nodes 13 and 15 (see Fig. 2) exhibits the classical behavior seen in most creep problems and the magnitude of these displacements is of the order of the wall thickness with an increasing rate. This result shows that the lateral pressure due to the sodium liquid column is the dominant loading effect.

As a sharp contrast, the results of cases (3a) and (3b) exhibit a degree of static stability and independence of the creep phenomena. The case (3a) model is identical in structural loading to case (2a); however, the thermal boundary condition on thermal load line 5 of Fig. 3, is changed. We assumed that for both cases (3a) and (3b) a wall cooling system can be furnished so that the outer surface of the cavity wall is exposed to a ramp-type temperature increase from 100°C to 250 °C. The temperature profiles in the radial direction reach the expected linear variation from 900°C on the inside surface to 250°C on the outer surface, while the majority of the material in the cavity wall is at a sufficiently low temperature in order to maintain structural integrity.

The case (3b) was intended to be identical to case (3a) except that once again the weight of the reactor assembly was removed from the cavity wall. The results calculated for case (3b) turn out to be nearly identical to those of case (3a) showing again that the temperature variation through the lower part of the cavity wall is the critical phenomenon.

We believe that the success shown for cases (3a) and (3b) should demonstrate that furnishing a cooling system for the cavity wall outer surface is most critical in order to overcome the thermal-stress problems associated with this wall.

References

[1] SCHREYER, H. L., KENNEDY, J. M., SCHOEBERLE, D. F., "Thermo-Viscoplastic Analysis of First Walls Subjected to Fusion Power Transients," Journal of Pressure Vessel Technology, 105, pp. 42-50 (1983).

[2]   KENNEDY, J. M., BELYTSCHKO, T., SCHOEBERLE, D. F., "STRAW - a Nonlinear Fluid-Structural
      and Thermo-Mechanical Finite Element Program," ANL-85-4, Argonne National Laboratory,
      (February, 1985).

[3]   DIMELFI, R. J., KRAMER, J. M., "Modelling the Effects of Fast Neutron Irradiation on the
      Subsequent Mechanical Behaviour of Type 316 Stainless Steel," Journal of Nuclear
      Materials, 89(2,3), pp. 338-346 (1980).

[4]   Metals Handbook, American Society for Metals, 8th Edition, Vol. 1.

[5]   CROSSLAND, B., PATTON, R. G., SKELTON, W. J., "The Comparison of Torsion and Tension
      Creep Data for a 0.18% Carbon Steel," in Advances in Creep Design, edited by A. I. Smith
      and A. M. Nicolson, Halsted Press Division, New York, pp. 129-150 (1971).

[6]   TARIA, S., OHTANI, R., "Creep in Tubular Specimens under Combined Stress," in Advances
      in Creep Design, edited by A. I. Smith and A. M. Nicolson, Halsted Press Division, New
      York, pp. 289-328 (1971).

Table I. Material Properties, Low Carbon Steel

Density	ρ = 7780	kg/m^3
Poisson's Ratio	ν = 0.3	
Coefficient of Thermal Expansion	α = 1.275 (10^{-5})	
Thermal Conductivity	k = 39.1	Watts/m-°C
Specific Heat	C_p = 695.0	Joules/Kg-°C
Modulus of Elasticity	E = 1.895 x 1-^{11}	Pascals for T_o = 100°C
for T > 100°C	E = 2.0G (1+ν)	
where	G = Shear Modulus calculated internally	

Table II. Results of Thermal Stress Analyses

Case	Reactor Weight on Node 39 (tons)	Thermal Boundary Condition Load Lines	Max Radial Disp Node 13 Meters	Max Radial Disp Node 15 Meters	Max Plastic Strain in Cavity Wall (%)
2a,2b	3330	Adiabatic	1.46	1.75	21.8
2c	0.0	Adiabatic	0.180	0.215	2.59
3a	3330	Ramp-type rise	0.0387	0.0421	2.35
3b	0.0	Ramp-type rise	0.0387	0.0424	2.09
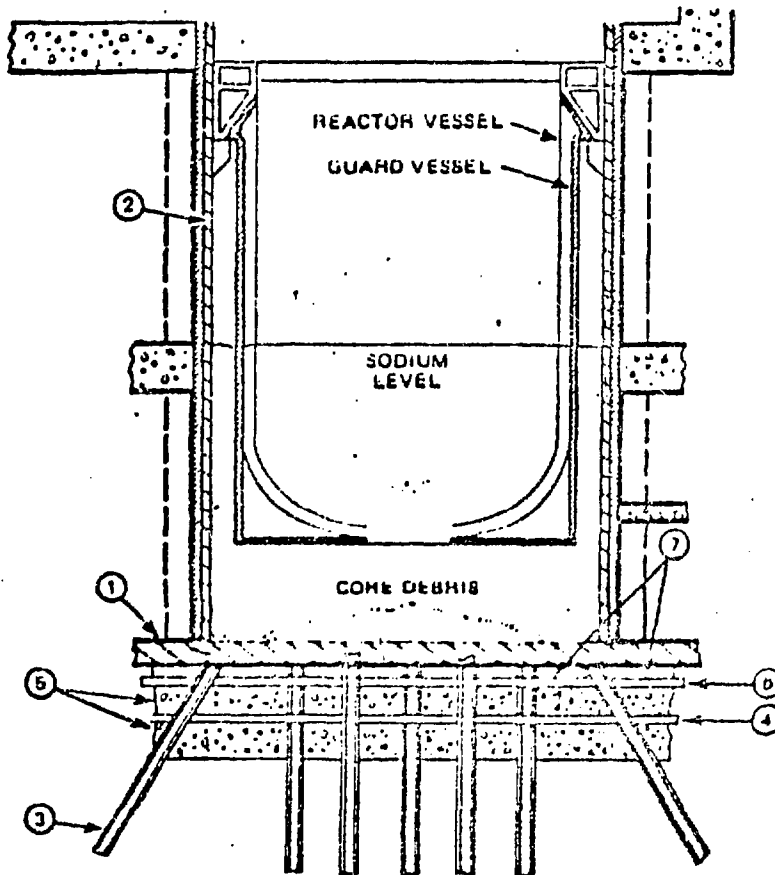
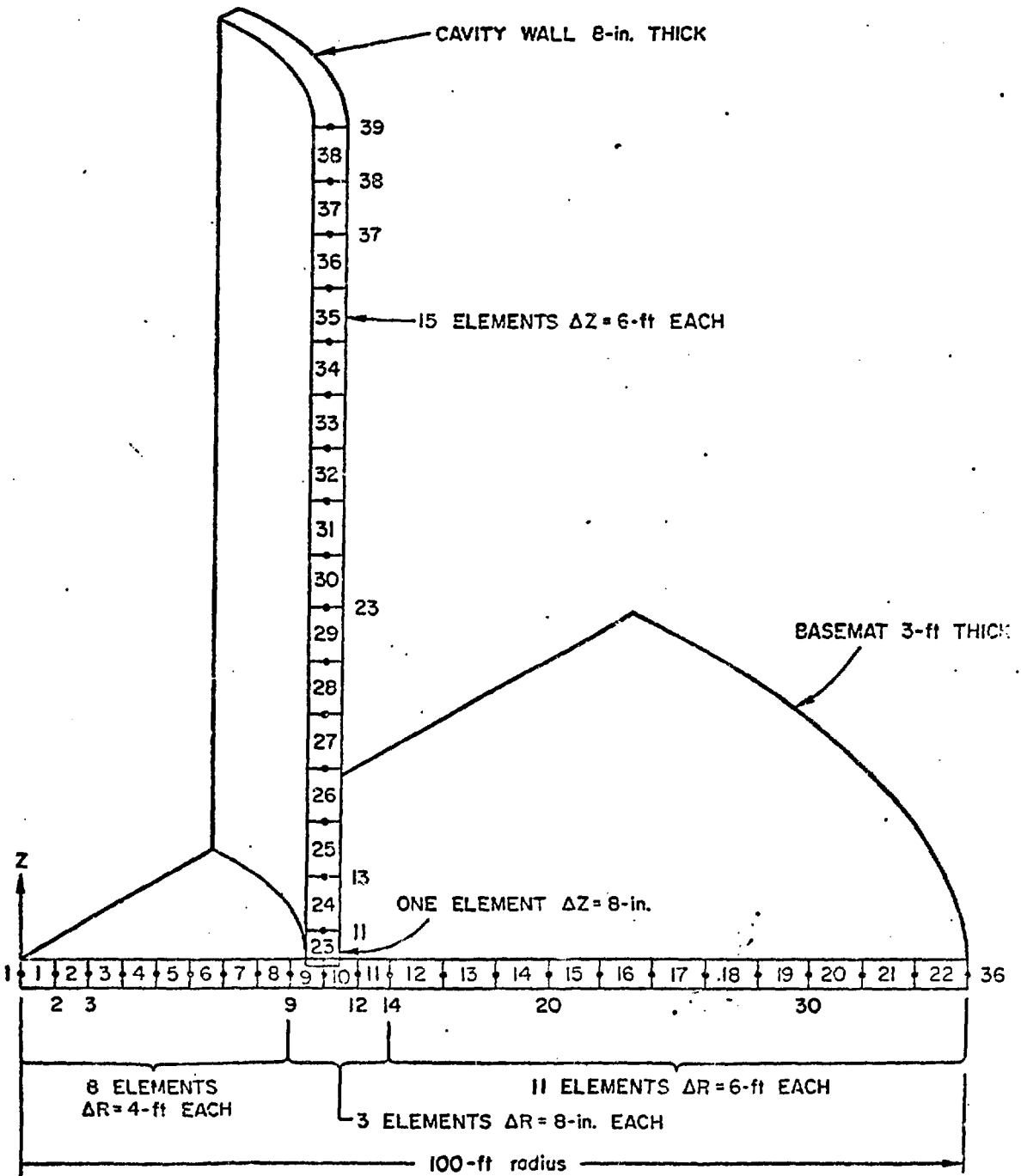Fig. 1. General Electric metal basemat concept.
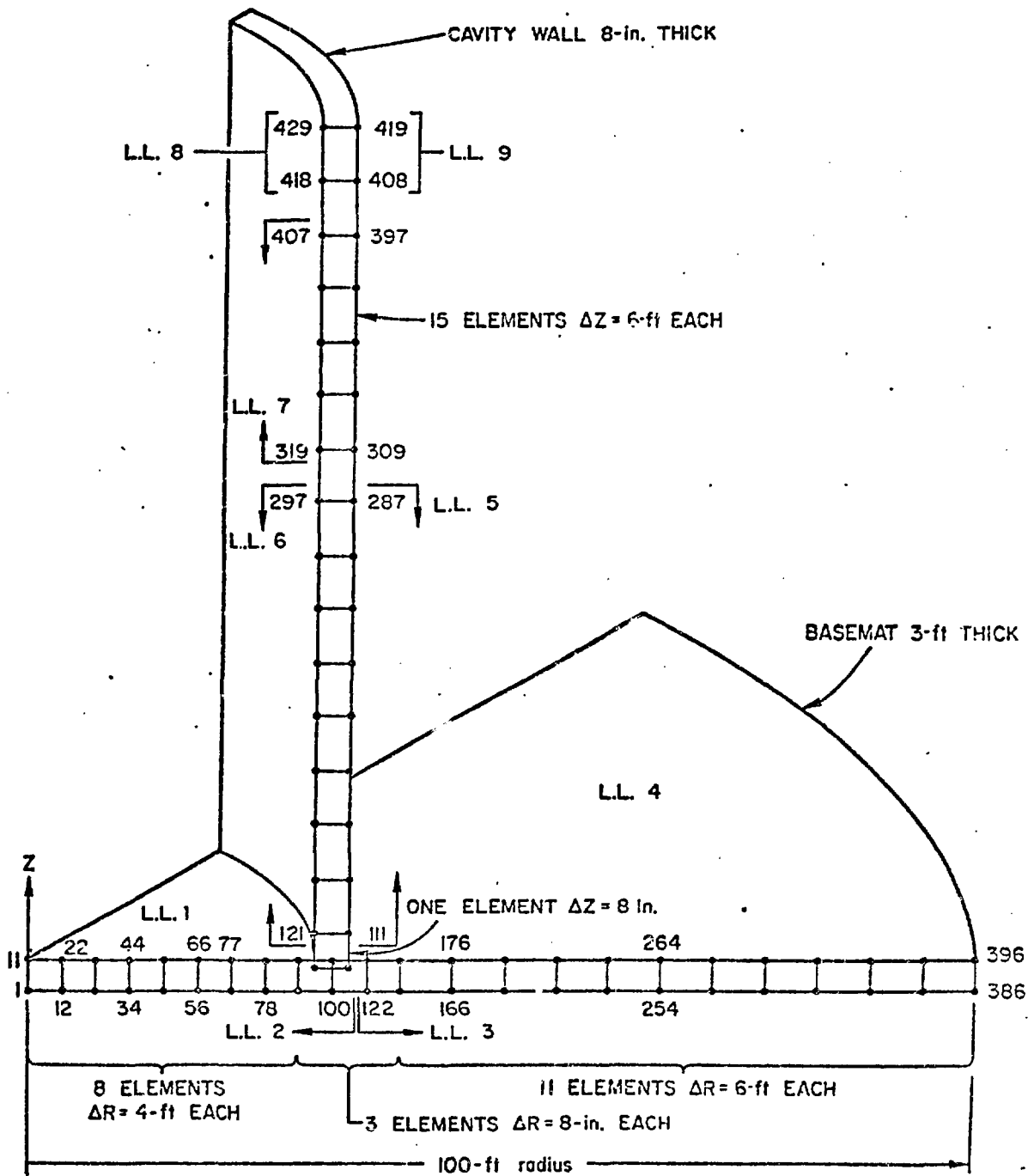
Fig. 2. Structural finite element mesh.

Fig. 3. Thermal finite element mesh (10 thermal elements per structural element).